



Originally published as:

Stadtlander, R., Mechie, J., Schulze, A. (1999): Deep structure of the southern Ural mountains as derived from wide-angle seismic data. - *Geophysical Journal International*, 137, pp. 501—515.

DOI: <http://doi.org/10.1046/j.1365-246X.1999.00794.x>

Deep structure of the southern Ural mountains as derived from wide-angle seismic data

R. Stadtlander, J. Mechie* and A. Schulze

GeoForschungsZentrum Potsdam (GFZ), Department 2, Telegrafenberg, 14473 Potsdam, Germany

Accepted 1998 November 29. Received 1998 November 24; in original form 1998 March 4

SUMMARY

P- and *S*-wave modelling of the data obtained during the seismic refraction–wide-angle reflection experiment of the URSEIS95 project demonstrate the presence of a 15–18 km thick crustal root beneath the Magnitogorsk-Tagil zone in the central part of the Urals orogen. However, the centre of this crustal root is displaced by 50–80 km to the east of the present-day maximum topography. Also beneath the Magnitogorsk-Tagil island arc zone, an upper crustal body with a high *P*-wave velocity of 6.3 km s⁻¹ at 4–9 km depth can be interpreted as consisting of mafic and/or ultramafic rocks. This, in turn, would help to explain the positive Bouguer gravity anomaly and the surface heat-flow minimum associated with the zone, and would also be consistent with the known surface geology of the zone. Another major feature of the seismic model is the presence of high *P*- and *S*-wave velocities (7.5 and 4.2 km s⁻¹, respectively) at the base of the crustal root. If the deeper parts of the thickened crust also have high densities (small density contrast of about -0.1 g cm⁻³ with respect to the uppermost mantle) then this helps to explain the absence of a pronounced gravity minimum associated with the root. These high velocities and densities can be most easily explained by mafic rocks or a mix of mafic and ultramafic rocks. Within the structural framework of Berzin *et al.* (1996) these rocks would belong to the lower Russian plate, which was being subducted beneath the Siberian plate during the Uralian orogeny. It is possible that the crustal root is formed from the remnants of oceanic crust or a mix of oceanic crust and mantle attached to the Russian plate. This would mean that little or no continental crust has been subducted or that subduction, and hence the Uralian orogeny, stopped when there was no more oceanic crust or when an attempt was made to subduct lighter continental crust.

Key words: crustal structure, Russia, seismic refraction, Ural mountains.

INTRODUCTION AND EXPERIMENT DESCRIPTION

The Urals are a mid to late Palaeozoic orogenic belt which today forms the boundary between Europe and Asia. In contrast to other mountain belts of similar age, for example the Variscides (Bois 1991; Aichroth *et al.* 1992) or Appalachians (Cook *et al.* 1981; Nelson 1992), which appear to have no crustal root preserved beneath them, there is evidence from previous seismic investigations (for example Egorkin & Mikhaltsev 1990; Ryzhiy *et al.* 1992; Thouvenot *et al.* 1995; Ryberg *et al.* 1996) that at least in some places there is a crustal root preserved beneath the Urals. During the summer of 1995, a multinational group of geoscientists from Russian, German, American and Spanish institutions carried out a large-

scale seismic project, URSEIS95, across the southern Urals with the major aim of identifying the presence of a crustal root beneath this portion of the mountain belt (for preliminary reports see Berzin *et al.* 1996; Carbonell *et al.* 1996; Echtler *et al.* 1996; Knapp *et al.* 1996). The purpose of this article is to describe in detail the results obtained from *P*- and *S*-wave modelling of the data obtained during the seismic refraction–wide-angle reflection experiment which was one of the three components of the URSEIS95 seismic project. The other two components comprised a near-vertical incidence vibroseis reflection survey and a near-vertical incidence explosive-source reflection survey.

In June 1995, as part of the URSEIS95 project in the southern Ural mountains, a seismic refraction–wide-angle reflection experiment involving a total of six deployments, was carried out (Fig. 1). During the first deployment, a N–S line along the 60°E meridian was completed. A shot was fired at

*Corresponding author.

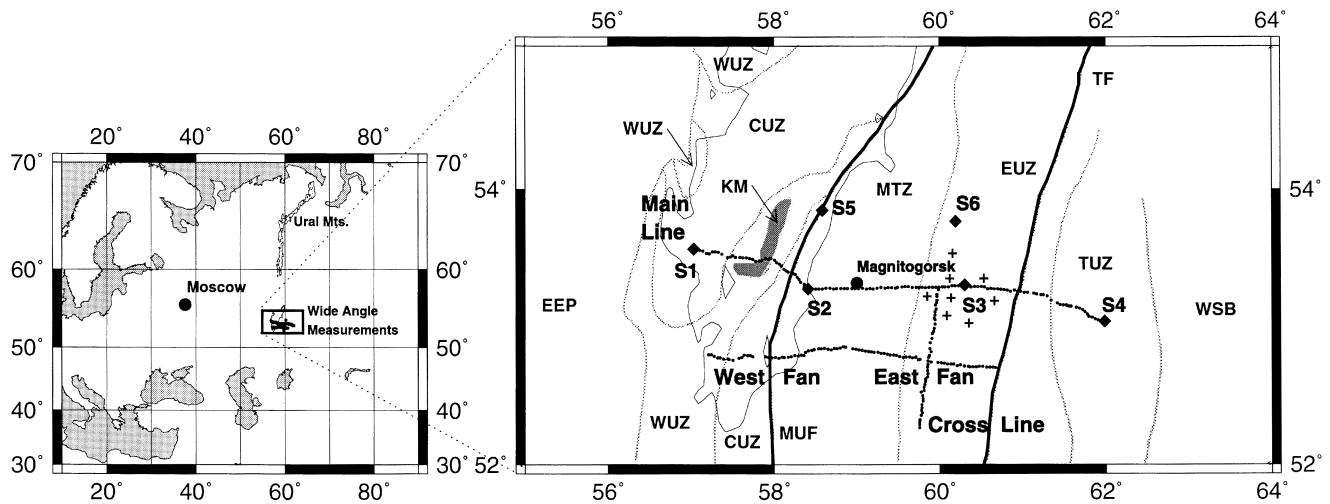


Figure 1. Location and simplified geological map. The diamonds show the position of the shot-points S1–S6, while the heavy dotted lines represent the recording sites. The heavy black lines show the traces of the Main Uralian Fault (MUF) and the Troitsk Fault (TF), and the light dotted lines show the outlines of the main tectonic zones (after Berzin *et al.* 1996). The light continuous line defines the 500 m contour. EEP: East European Platform; WUZ: West Uralian Zone; CUZ: Central Uralian Zone; KM: Kraka Massif; MTZ: Magnitogorsk-Tagil Island Arc Zone; EUZ: East Uralian Zone; TUZ: Trans Uralian Zone; WSB: West Siberian Basin; +: Dzshabic granite.

shot-point 6 and recorded by 50 stand-alone three-component instruments with an average spacing of about 2.4 km, southwards from the cross-point with the E–W main line for about 120 km. This N–S cross-line was sited about 100 km east of the 500 m contour defining the present-day topographic expression of the Ural mountains, in the East Uralian zone. With the second and third deployments, fan profiles were recorded. The first fan deployment constituted the firing of a shot at shot-point 6 and the recording of the seismic waves by the 50 instruments along the 115 km long eastern fan at an average spacing of 2.3 km. The second fan deployment involved the firing of a shot at shot-point 5 and the recording of the seismic waves by the 50 instruments along the 115 km long western fan, again at an average spacing of 2.3 km. The fans were designed so that the reflection points would lie below the E–W main line. As shot-points 5 and 6 were approximately 60 km north of the E–W main line, this necessitated that the instruments be situated about 60 km south of the E–W main line. About half of the western fan was situated west of the Main Uralian Fault in the West and Central Uralian zones, while the other half of the western fan and the whole of the eastern fan were sited east of the Main Uralian Fault in the Magnitogorsk-Tagil island arc zone and the East Uralian zone. The majority of the recording stations of the western fan were sited above the 500 m contour of the Ural mountains.

The major effort of the wide-angle experiment involved a 335 km long E–W main profile (Fig. 1). This profile was coincident with the eastern 335 km of the 465 km long URSEIS95 near-vertical incidence reflection profile. The profile was completed in deployments four to six. In the fourth deployment, the 50 instruments were placed between shot-points 2 and 4 with an average spacing of 4.6 km and shots were fired at shot-points 2, 3 and 4. In the fifth deployment, the instruments were moved by half of the station spacing and shots were fired at shot-points 1, 2, 3 and 4. In the sixth and final deployment, the 50 instruments were placed between shot-points 1 and 2 at an average spacing of around 2.3 km and shots were fired at shot-points 1–4. Thus, for shot-points 2–4 an average

instrument spacing of 2.3 km was realized along the whole line. For shot-point 1 an average spacing of 2.3 km was achieved between shot-points 1 and 2, while between shot-points 2 and 4 the average spacing was 4.6 km. Shot-point 1 was located about 80 km west of the Main Uralian Fault in the Central Uralian zone. That part of the E–W main profile between shot-points 1 and 2 crosses the present-day topographic expression of the Ural mountains, with station heights above 500 m. Shot-point 2 lay about 20 km east of the Main Uralian Fault in the Magnitogorsk-Tagil island arc zone. Shot-point 3 was situated about 120 km east of the 500 m contour of the Ural mountains near the edge of the Dzshabic granite in the East Uralian zone, while shot-point 4 was located about 80 km east of the Troitsk fault in the Trans Uralian zone.

The major aim of the E–W main line was to delineate the Moho (crust–mantle boundary) structure beneath the line and thus identify the presence of a crustal root beneath this part of the mountain belt and, if present, to determine the depth of such a root. A further goal of the E–W main line was to derive estimates of crustal *P*-wave velocities and, as the measurements were being made with three-component instruments, also *S*-wave velocities, in an attempt to place constraints on the rock types beneath the orogen and in particular in the crustal root, if present. A third reason for completing the E–W main line was to provide velocity control for the near-vertical incidence reflection profile by means of a 2-D velocity–depth model along the line. The main purpose of the N–S cross-line was to determine crustal velocities and structure parallel to the trend of the mountain belt, to see if there were any large-scale differences with respect to the E–W main line. The main purpose of the fan profiles was to detect major E–W variations in the main structural interfaces, especially the Moho.

THE E–W MAIN LINE

P-wave sections

Figs 2–5 show, for each of the shot-points 1–4 along the E–W main line, the compressional (*P*) seismic wavefield recorded by

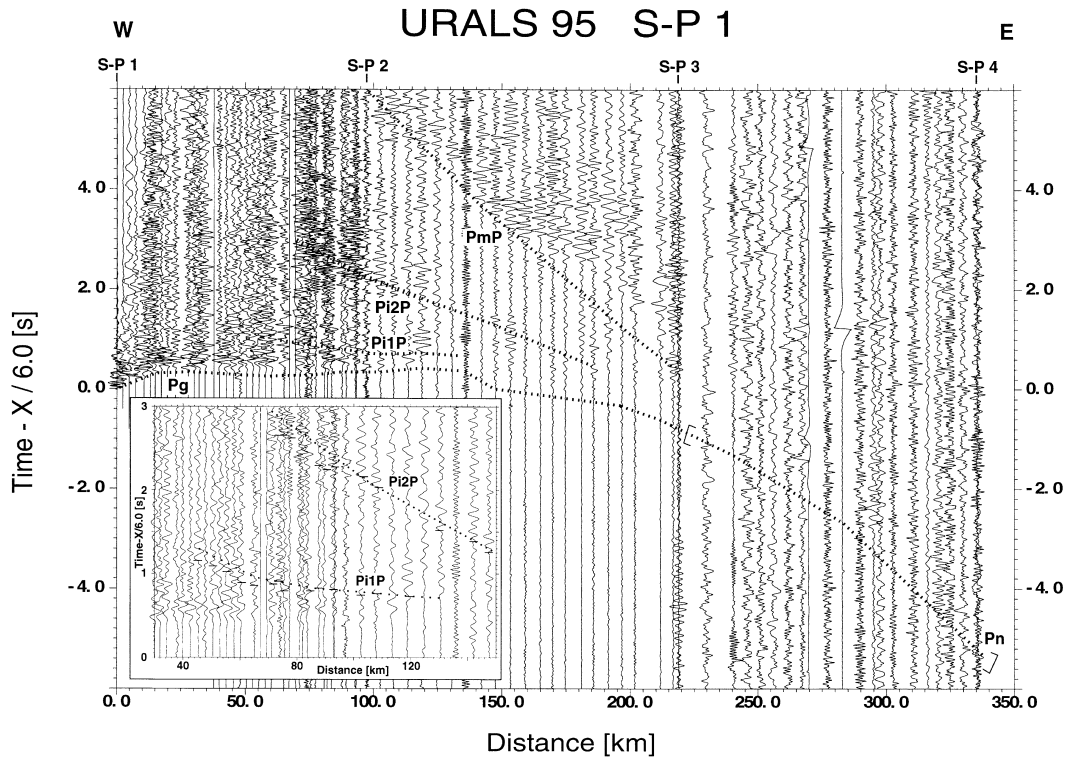


Figure 2. Seismic data from shot-point 1 along the URSEIS 95 E–W main line. The record section reduced with a velocity of 6 km s^{-1} shows the vertical component of P -wave motion in which each trace is normalized individually and bandpass filtered from 1 to 20 Hz. Dotted lines represent phases calculated from the model in Fig. 7, and dotted lines in [] represent phases calculated from the model in Fig. 7 but for which there is little or no evidence in the section. P_g : first-arrival refraction through the upper crust; P_{i1P} : reflection from the top of the middle crust; P_{i2P} : reflection from the top of the lower crust; P_{mP} : reflection from the Moho; P_n : first-arrival refraction through the uppermost mantle. The inset contains an expanded-scale portion of the section showing the comparison between the observed (horizontal ticks) and calculated (continuous dotted line) P_{i1P} and P_{i2P} traveltimes.

the vertical component of the instruments at each receiver position. These shot gathers are displayed in the form of distance versus reduced-time record sections, in which each trace has been bandpass filtered (1–20 Hz) and normalized with respect to its own maximum amplitude. The reduction velocity is 6 km s^{-1} . Traveltimes calculated from the derived model (Figs 6 and 7) are drawn in on the record sections.

Apart from the last 110 km from shot-point 1, the data are of very good quality with correlatable arrivals out to the maximum recording distances from shot-points 2–4. The record sections, however, show different features in the recorded wavefields. For example, the section from shot-point 1 (Fig. 2) shows a well-defined P_{mP} phase (wide-angle reflected phase from the Moho) between 110 and 210 km distance, with sharp onsets and amplitudes well above the preceding signal. In contrast, the section from shot-point 3 recorded to the west (Fig. 4) is dominated by a reverberating signal which starts within 0.5 s of the first arrival and does not allow the identification of later secondary arrivals with any great certainty.

In addition to the bright P_{mP} phase in the record section from shot-point 1, clear, even if sometimes relatively small, first arrivals can be observed out to around 210 km distance (Fig. 2). At distances less than 15 km the apparent velocity of the first arrivals is about 5.5 km s^{-1} . Between 15 and 140 km distance the average apparent velocity of the first arrivals is about 6 km s^{-1} and these arrivals can be safely assigned to

the P_g phase, the refracted phase through the upper crust. One significant departure from the average apparent velocity close to 6 km s^{-1} can be seen between 115 and 140 km distance, where the first arrivals are somewhat delayed. This traveltimes delay at this location along the main line can be seen more prominently in the record section from shot-point 2. Beyond about 140 km distance, the average apparent velocity of the first arrivals is significantly greater than 6 km s^{-1} (6.4 km s^{-1}) and the question is whether these arrivals are from the upper crust or from deeper crustal levels. This question will be returned to when the model is discussed below. It is possible to distinguish two intracrustal reflected phases on the record section from shot-point 1. The earlier (P_{i1P}) can be identified just behind the P_g phase on some traces between 45 and 120 km distance. The second (P_{i2P}) can be observed between about 70 and 150 km distance and 1–3 s reduced time (Fig. 2, inset).

The record section from shot-point 2 shows distinct although often small first arrivals out to both ends of the line (Fig. 3). Towards the west, the first arrivals have an apparent velocity of about 5.6 km s^{-1} out to about 25 km distance. Beyond this distance, despite the somewhat undulatory nature of the arrival times, the average apparent velocity is close to 6.0 km s^{-1} and the arrivals belong to the P_g phase. Towards the east, the apparent velocity of the first arrivals is about 5.5 km s^{-1} out to about 35 km distance and is significantly greater than 6.0 km s^{-1} (around 6.6 km s^{-1}) between 35 and 65 km distance. This pattern in the first arrival times may be thought of as a

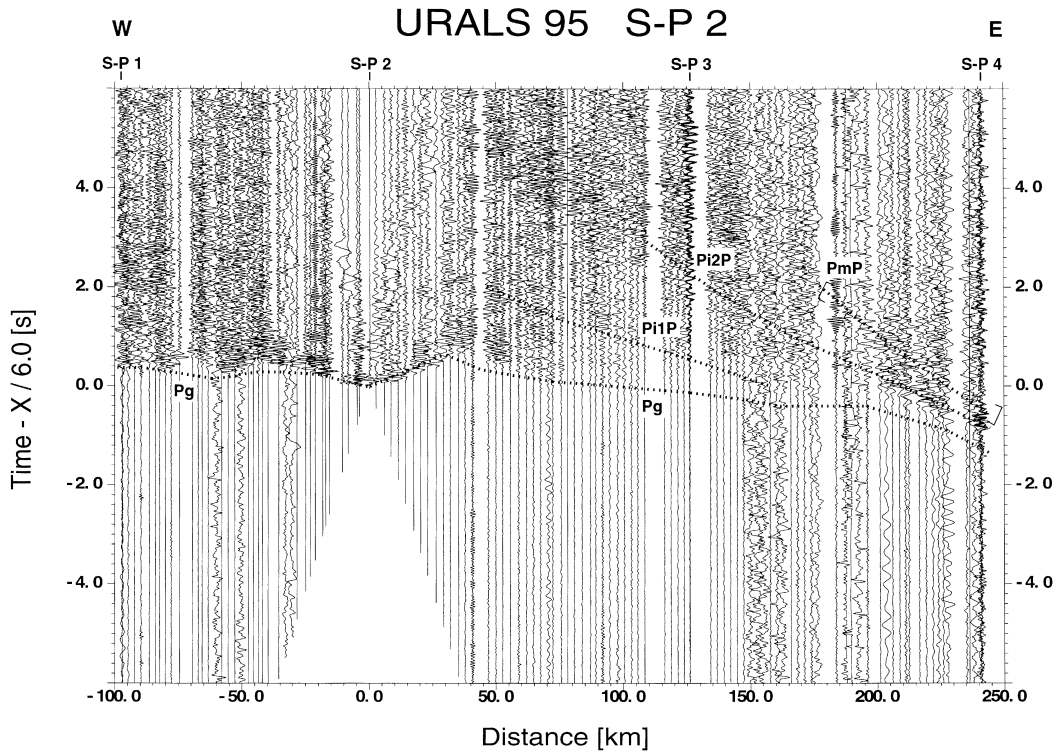


Figure 3. Vertical-component *P*-wave record section from shot-point 2 along the URSEIS 95 E–W main line. The data are processed and presented as in Fig. 2. Key: see Fig. 2.

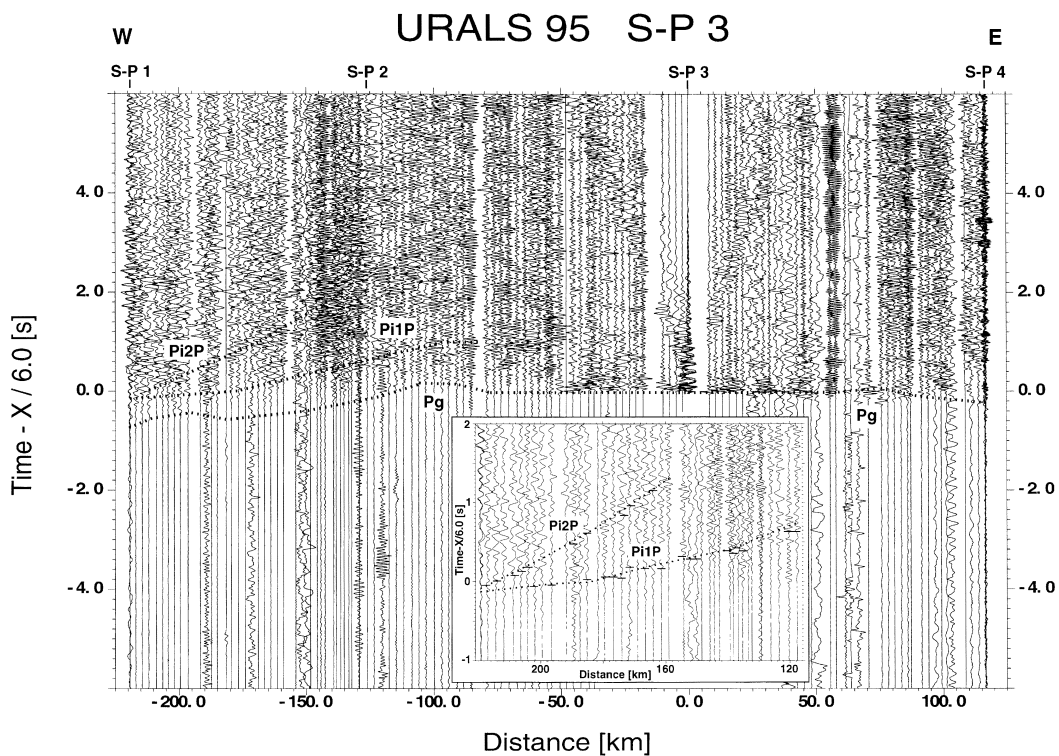


Figure 4. Vertical-component *P*-wave record section from shot-point 3 along the URSEIS 95 E–W main line. The data are processed and presented as in Fig. 2. Key: see Fig. 2. The inset contains an expanded-scale portion of the section showing the comparison between the observed (horizontal ticks) and calculated (continuous dotted line) Pi1P and Pi2P traveltimes.

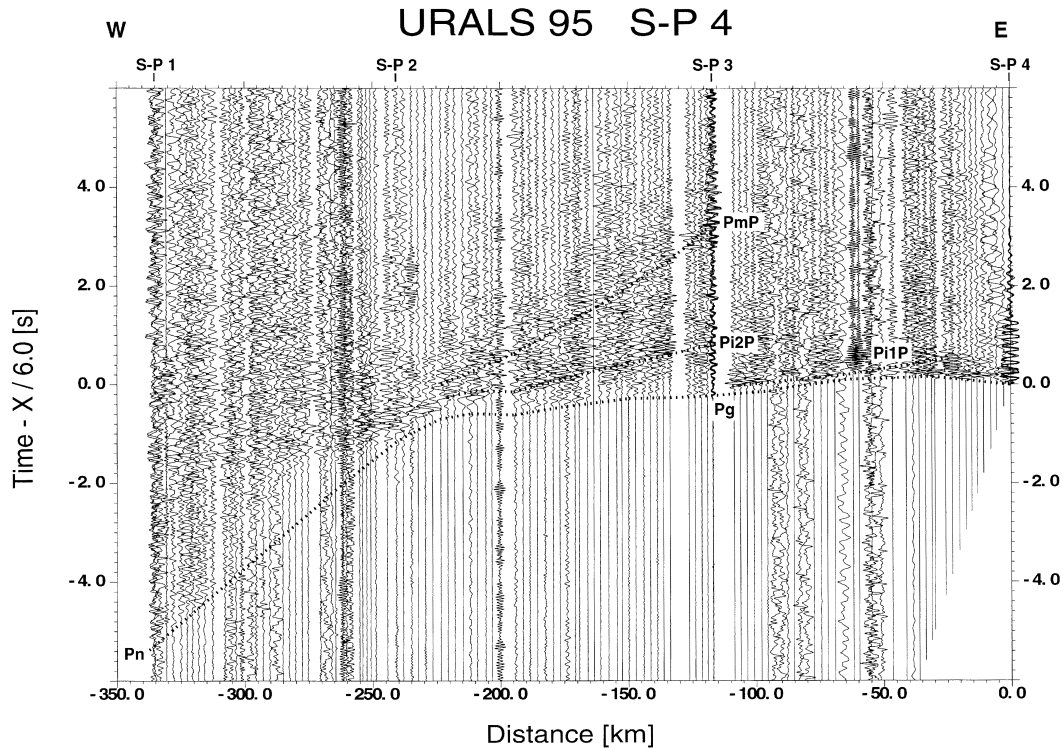


Figure 5. Vertical-component *P*-wave record section from shot-point 4 along the URSEIS 95 E–W main line. The data are processed and presented as in Fig. 2. Key: see Fig. 2.

delay centred around 35 km east of shot-point 2 and is in the same location as the delay which was observed with somewhat smaller effect in the record section from shot-point 1. Between 65 and 200 km the first arrivals have an apparent velocity of about 6.1 km s^{-1} and can be identified as the *Pg* phase. Beyond 200 km distance, the first arrivals have an apparent velocity significantly greater than 6.0 km s^{-1} (around 6.5 km s^{-1}) and probably have their turning points in the middle crust. Towards the east the most prominent reflection on this record section is the intracrustal phase *Pi2P*. It can be recognized between 50 and 200 km distance, not so much by sharp onsets as in the case of the *PmP* phase on the section from shot-point 1, but rather by an increase in energy level. This increased energy level has a rather long time duration and thus masks the expected arrival times of the *PmP* phase, which as a consequence is not observed on the section. Between the first arrivals and the *Pi2P* phase, another intracrustal reflected phase, *Pi1P*, can be seen on some traces between 50 and 150 km distance and between 0 and 2 s reduced time.

On the record section from shot-point 3 (Fig. 4) the apparent velocity of the first arrivals close to the shot-point is around 6.0 km s^{-1} , and thus the first arrivals out to the end of the line towards the east and those out to about 120 km to the west belong to the *Pg* phase. Between about 85 and 115 km distance to the west, a small delay in the first arrivals can be recognized, occurring at the same location as the delays centred at about 35 km east of shot-point 2 and 130 km east of shot-point 1. Beyond 120 km distance the first arrivals have an average apparent velocity of $6.2\text{--}6.3 \text{ km s}^{-1}$ and thus could have turning points in the middle crust. This is the record section most dominated by reverberating signals and thus the identification of secondary arrival phases has proved to be difficult. Towards

the west between 120 and 200 km distance and between -0.5 and 1 s reduced time, an intracrustal reflected phase, *Pi1P*, can be identified. This phase is accompanied by the first and most prominent increase in energy level which occurs in this record section and which marks the beginning of the reverberating signal in this part of the section. Behind the *Pi1P* phase some arrivals corresponding to the *Pi2P* phase can possibly be picked (Fig. 4, inset).

Shot-point 4 provided the record section with the most information (Fig. 5). The *Pg* phase forms the first arrivals out to 200 km distance, with average apparent velocities of about 5.9 km s^{-1} out to 30–40 km distance and around 6.1 km s^{-1} beyond this distance. Beyond 200 km distance the *Pn* phase forms the first arrivals, with strong relative amplitudes compared to other phases beyond 300 km distance. The average apparent velocity of the *Pn* phase is 7.75 km s^{-1} . Between 115 and 130 km distance some relatively strong *PmP* arrivals can be recognized. At this distance the average apparent *Pn* velocity is asymptotic to these *PmP* arrivals and thus the critical point of the *PmP* phase must occur at about this distance. At distances beyond 130 km the *PmP* phase is marked by an increase in energy level. The most prominent reflected phase on this section is the intracrustal phase *Pi2P*, which can be correlated between 100 and 220 km distance and between -0.5 and 1 s due both to quite sharp onsets and to a significant amplitude increase. Another intracrustal reflected phase, *Pi1P*, can be identified just behind the *Pg* phase on some traces between 30 and 100 km distance.

The reduced reciprocal traveltimes of the *Pn* phase between shot-points 1 and 4 is -5.3 s . If this point is plotted in the record section for shot-point 1 and a line is drawn through this point such that it is also asymptotic to the *PmP* phase

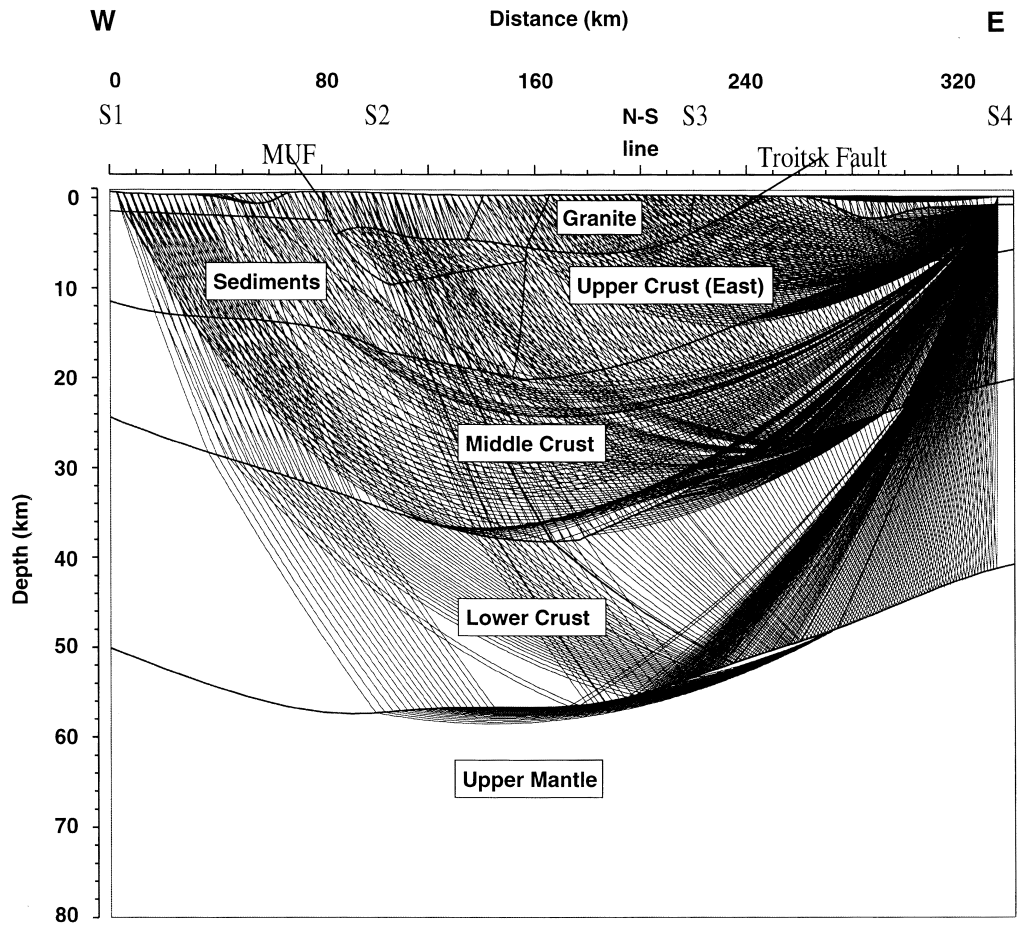


Figure 6. Ray diagram showing rays traced from shot-point S4 through the P -wave velocity model (see also Fig. 7) for the E–W main line.

then the critical point of the PmP phase occurs at 100–150 km distance and the average apparent velocity of the Pn phase is 8.3 km s^{-1} . Thus the apparent Pn velocity from shot-point 4 can be viewed as a down-dip apparent velocity, and that from shot-point 1 as an up-dip apparent velocity, in which case the true velocity of the Pn phase would be about 8.0 km s^{-1} and the Moho depth below shot-point 1 would be greater than that under shot-point 4. That the Moho is deeper beneath shot-point 1 than below shot-point 4 can also be deduced from the arrival times of the PmP phase near the critical point on the two sections. The reduced traveltimes of the PmP phase at 120 km distance on the section from shot-point 4 is 2.8 s (Fig. 5), while that on the section from shot-point 1 is 4.7 s (Fig. 2). This 1.9 s difference in arrival times, in addition to the apparent Pn velocities, provides the first indication that a crustal root exists in some form beneath the Urals, as shot-point 1 was sited in the mountains themselves while shot-point 4 was sited on the plains to the east of the Urals (Fig. 1).

P -wave model

A 2-D model for the E–W main line was derived by trial-and-error forward modelling using the ray-tracing facility in the GX II (GX II is a Trademark of GX Technology Corporation) commercial software modelling package (Fig. 6). As the upper crustal structure in the model is fairly complicated, the first arrival traveltimes were also calculated using a finite-difference

approximation of the eikonal equation (Vidale 1988; Podvin & Lecomte 1991; Schneider *et al.* 1992). Amplitudes were calculated using a finite-difference formulation of the wave equation for 2-D heterogeneous elastic media by Kelly *et al.* (1976) with transparent boundary conditions (Reynolds 1978) and implemented by Sandmeier (1990).

Modelling of the upper crustal structure along the E–W main line involved mainly the fitting of the first-arrival traveltimes out to about 150–200 km distance. In doing this, an attempt was made to take into account the complicated geology. West of the Main Uralian Fault (MUF) in the West and Central Uralian zones, a layer with a velocity of $6.0\text{--}6.1 \text{ km s}^{-1}$ is overlain by a 2–3 km thick cover layer with a velocity of around 5.5 km s^{-1} (Fig. 7). In the region of the Kraka ophiolite massif between model kilometres 40 and 70, a thin surface layer with a velocity of about 6.2 km s^{-1} has been included. The West and Central Uralian zones occupy the footwall of the Main Uralian Fault and consist of a fold and thrust belt in which a 2–3 km thick section of Palaeozoic rocks overlies a 12–15 km thick section of Vendian and Riphean rocks which in turn overlie Archaean crystalline basement rocks (Brown *et al.* 1996). Although part of the recording line between shot-points 1 and 2 is situated on Palaeozoic rocks, shot-point 1 and the westernmost 30 km of the recording line are sited on Riphean sediments. Thus the 5.5 km s^{-1} layer must represent in part Riphean sediments as well as Palaeozoic rocks. It is possible that the boundary at 10–20 km depth

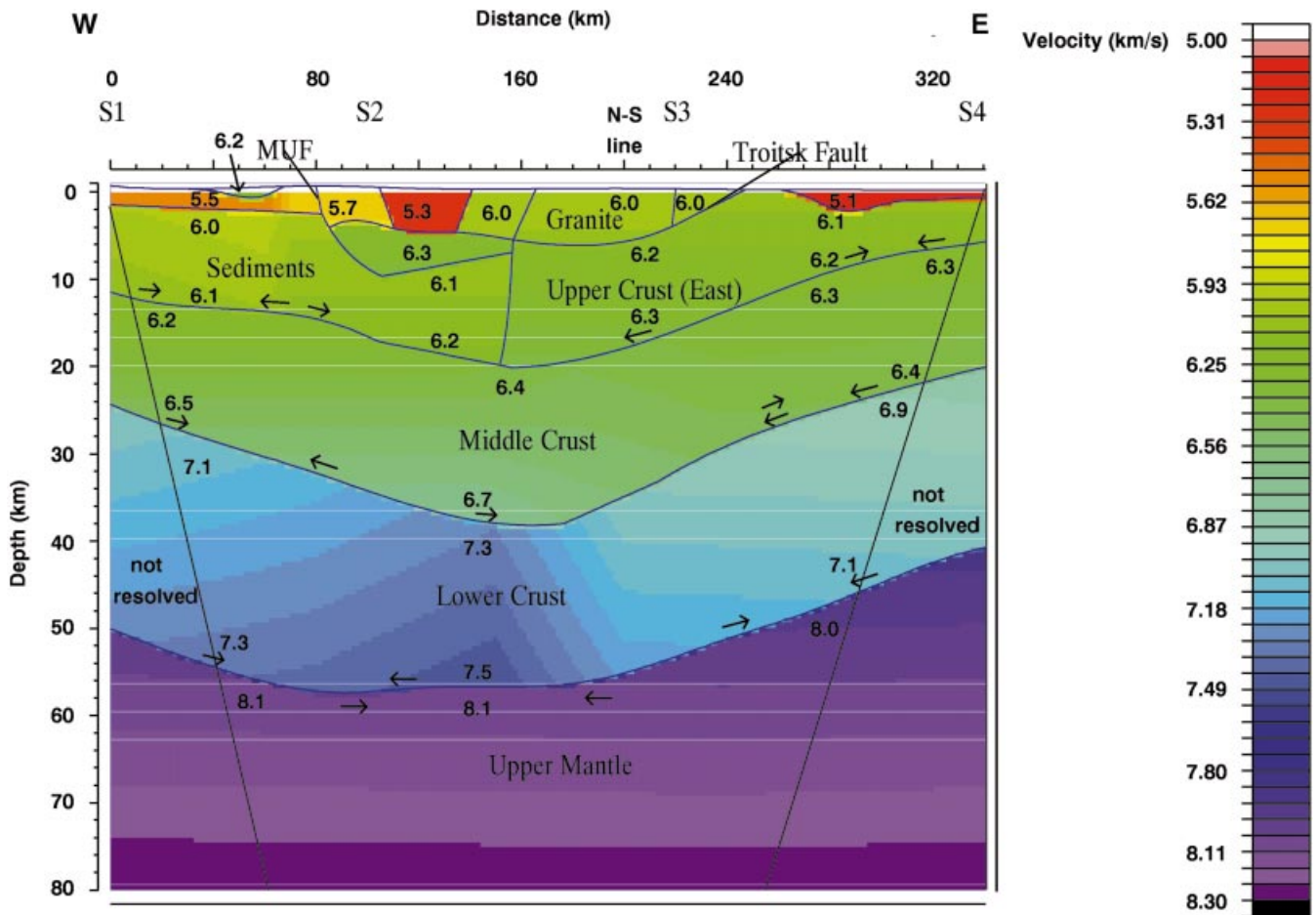


Figure 7. *P*-wave velocity model for the E–W main line. Velocities are in km s^{-1} . The regions between the arrowheads delineate those portions of the boundaries substantiated by reflected phases (arrows above the boundaries) or refracted phases (arrows below the boundaries) observed in the data. S1–S4: shot-points S1–S4. MUF: Main Uralian Fault.

in the western part of the profile corresponds to the top of the Archaean basement. The $6.0\text{--}6.1 \text{ km s}^{-1}$ layer would then mainly correspond to the thick section of Vendian and Riphean sediments.

East of the Main Uralian Fault, in the Magnitogorsk-Tagil island arc zone (between model kilometres 80 and 160), a central area with a low velocity of 5.3 km s^{-1} flanked by two regions with higher velocities of $5.7\text{--}6.0 \text{ km s}^{-1}$ was modelled. These three units are underlain by a region with a velocity of 6.3 km s^{-1} . With this structure the first arrivals out to about 70 km east of shot-point 2 can be well fitted, as can the first arrivals in this region from the other shot-points, especially the delays centred at about 130 km east of shot-point 1 and about 100 km west of shot-point 3. The structure can be thought of as representing in a simplified manner the synformal structure of the Magnitogorsk-Tagil zone, with low velocities in the younger central part of the synform and high velocities in the older outer flanks. Whether the deeper unit with the higher velocity of 6.3 km s^{-1} represents the deeper parts of the synform structure or whether there is a structural boundary between this unit and the three overlying units is a matter for further examination.

In the East Uralian zone, east of the Magnitogorsk-Tagil zone, the profile mainly crosses the Dzshabic granite. In the

model, the surface units in this zone have been attributed a velocity of 6.0 km s^{-1} in accordance with the near-shot apparent velocities from shot-point 3. Based on evidence from the vibroseis CMP reflection profile (Echtler *et al.* 1996) the granitic unit has been truncated at about 6 km depth. East of the Troitsk Fault, in the Trans Uralian zone, a layer with velocities from 6.1 km s^{-1} at the top increasing to 6.2 km s^{-1} at the base is overlain by a thin cover layer with velocities of around 5.1 km s^{-1} . In this region, Russian geological maps show that the Ordovician to Carboniferous rocks are partly covered by Mesozoic and Cenozoic sediments.

The depths to the boundary marking the top of the middle crust (Fig. 7) have been determined by modelling of the earlier intracrustal reflected phase, *Pi1P*. The boundary occurs at 6–12 km depth beneath the ends of the profile and at about 20 km depth below the centre of the profile. It is associated with a velocity jump of up to 0.15 km s^{-1} and thus the velocity at the top of the middle crust layer varies from 6.2 to 6.3 km s^{-1} beneath the ends of the profile to about 6.4 km s^{-1} under the central part of the profile. Fitting of the traveltimes for the later intracrustal phase, *Pi2P*, has facilitated the determination of the depths to the top of the lower crust. At the ends of the profile the boundary between the middle crust and the lower crust occurs at 21–24 km depth, while beneath the centre of

the profile it occurs at 38–40 km depth. The velocities at the base of the middle crust vary from 6.4 to 6.5 km s⁻¹ at the ends, to about 6.7 km s⁻¹ beneath the centre of the profile.

On many seismograms, the first arrivals can be picked to within $\pm(0.05\text{--}0.1)$ s out to 200 km distance. These first-arrival data constrain the velocities down to about the base of the middle crust quite tightly, and perturbation of the model shows these velocities to be accurate to within ± 0.1 km s⁻¹. As a consequence, the depths to the top of the middle crust and the top of the lower crust are determined to an accuracy of $\pm(2\text{--}3)$ km, although the accuracy with which the reflected arrivals can be picked is $\pm(0.1\text{--}0.2)$ s at best.

The velocity contrast across the boundary between the middle crust and the lower crust is 0.5–0.6 km s⁻¹, and thus the top of the lower crust has velocities of 6.9–7.1 km s⁻¹ under the ends of the profile increasing to about 7.3 km s⁻¹ below the Magnitogorsk zone. Mainly through the analysis of the *PmP* and *Pn* arrivals, the Moho depth can be estimated. To the east of the Urals under shot-point 4, the near-vertical incidence reflection data provide evidence that the Moho occurs at about 13 s two-way traveltime, corresponding to almost 40 km depth (Echtler *et al.* 1996; Knapp *et al.* 1996). About 40–50 km west of shot-point 4, where the wide-angle data can first resolve the structure, the Moho occurs at around 46 km depth. Farther west the depths continue to increase until, beneath the

Magnitogorsk zone in the central part of the orogen, maximum Moho depths of about 58 km are reached. Towards the west end of the profile, Moho depths begin to decrease again. Farther west the near-vertical incidence reflection profile continues to document the decrease in crustal thickness until background values of about 40 km, corresponding to almost 13 s two-way traveltime, are reached some tens of kilometres west of shot-point 1 (Echtler *et al.* 1996; Knapp *et al.* 1996). Thus, in agreement with the *PmP* observations from shot-points 1 and 4 described above, the modelling shows the existence of a 15–18 km thick crustal root beneath the Magnitogorsk zone in the central part of the orogen. The centre of this crustal root occurs about 20–30 km east of shot-point 2 (Fig. 7) and is thus displaced by 50–80 km to the east of the area of the present-day maximum topography (Fig. 1). Velocities at the base of the crust range from 7.1 km s⁻¹ to 7.3 km s⁻¹ beneath the ends of the resolved portion of the profile to 7.5 km s⁻¹ beneath the Magnitogorsk zone. The uppermost mantle has been modelled with velocities of 8.0–8.1 km s⁻¹.

Synthetic seismograms have been calculated for the 2-D velocity model (Fig. 7) for all shot-points, and an example is presented for shot-point 4 (Fig. 8). In order to compute the synthetic seismograms and the first-arrival traveltimes using the finite-difference approximation of the eikonal equation, the 2-D velocity model was digitized with an 80 × 80 m grid

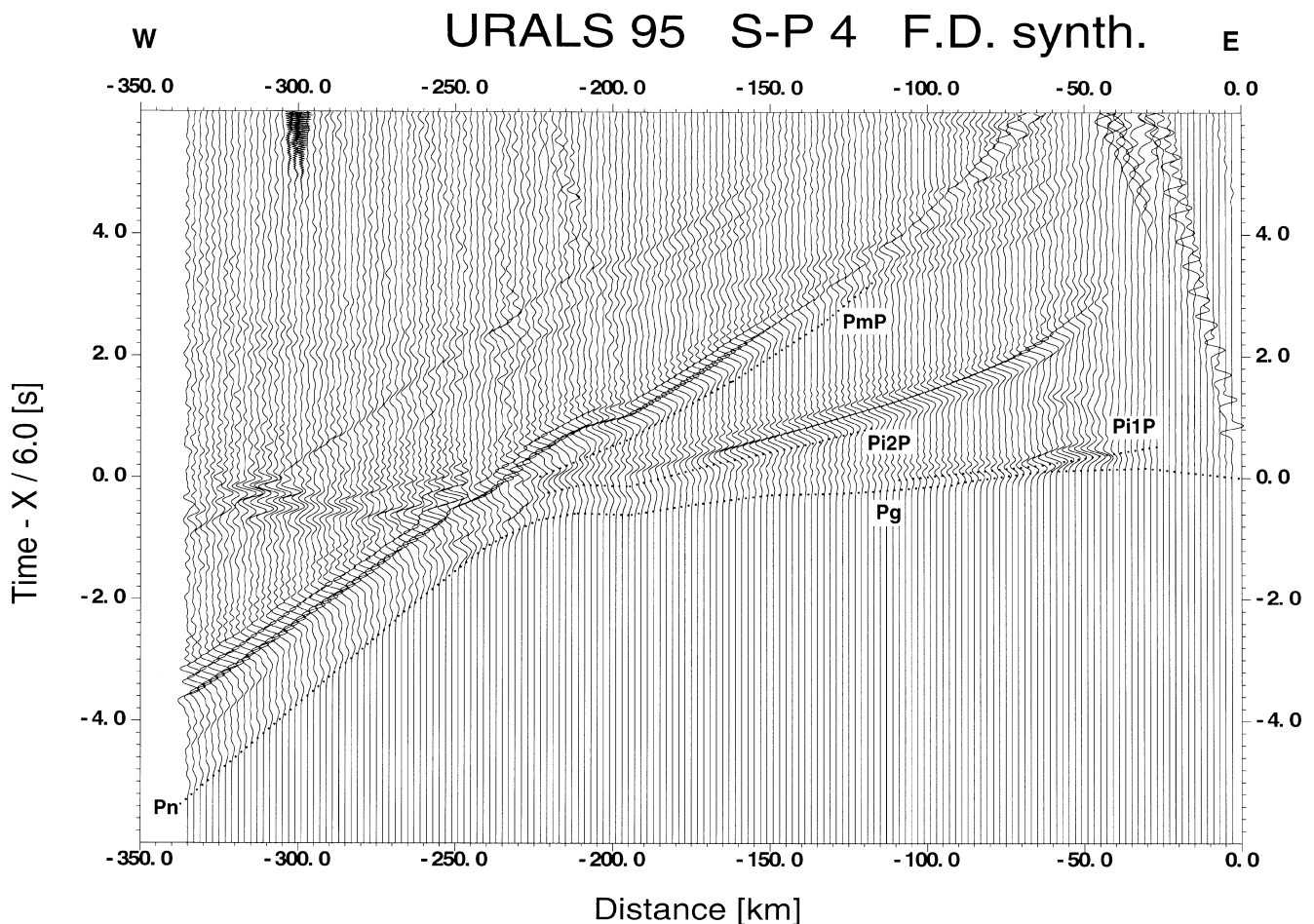


Figure 8. Synthetic seismogram section for shot-point 4 along the URSEIS 95 E–W main line. The section reduced with a velocity of 6 km s⁻¹ shows the vertical component of *P*-wave motion in which each trace is normalized individually. Dotted lines represent phases calculated from the model in Fig. 7. Key: see Fig. 2.

spacing. This in turn allowed the synthetic seismograms to be calculated for a dominant frequency of 3 Hz, which is somewhat lower than the dominant frequency of the observed seismograms. It is, however, high enough for the refractions and reflections from the relatively thick layers of the derived model to be calculated accurately. The relatively large velocity contrast of $0.5\text{--}0.6\text{ km s}^{-1}$ between the middle crust and the lower crust, and the resulting velocity contrast of $0.6\text{--}0.8\text{ km s}^{-1}$ across the Moho, means that in the synthetic seismograms the reflected phase, *Pi2P*, from the boundary between the middle crust and the lower crust is at least as prominent a phase as the reflected phase, *PmP*, from the Moho. This is in agreement with the observed data from shot-points 4 and 2. In the record section from shot-point 4 (Fig. 5), between distances of 100 and 200 km, the amplitudes of the reflection, *Pi2P*, from the boundary between the middle crust and the lower crust are about the same as those of the Moho reflection, *PmP*, while in the record section from shot-point 2 (Fig. 3), *Pi2P* is the dominant reflected phase and *PmP* is essentially not recognizable. However, the model does create a problem for shot-point 1 traces, which recorded a very bright *PmP* reflection. One possible explanation is that the velocity contrast across the boundary between the middle crust and the lower crust at the western end of the profile is somewhat smaller than that employed in the model (Fig. 7). Another possibility is that locally near the western end of the profile the velocity of the uppermost mantle is higher than the average value used in the model. A further feature which the synthetic seismograms fail to reproduce is the reverberatory nature of the observed seismograms between the major reflected phases, for example the coda energy which effectively masks the *PmP* reflection

behind the prominent *Pi2P* reflection in the record section from shot-point 2 (Fig. 3). This suggests that heterogeneities with short wavelengths possibly exist, especially in the middle crust and the lower crust under, in particular, the central and eastern parts of the profile. Despite the possible existence of such heterogeneities, it is thought that the average background (macro) velocities in the lower crust are accurate to within $\pm(0.2\text{--}0.3)\text{ km s}^{-1}$ and that the Moho depths are accurate to within $\pm(5\text{--}6)$ per cent.

S-wave sections

As examples, the shear (*S*) seismic wavefield recorded by the transverse component of the instruments at each receiver position is presented for shot-points 1, 2 and 4 along the E–W main line (Figs 9, 10 and 11). As with the *P*-wave data, the *S*-wave data are displayed as distance versus reduced-time record sections, in which each trace has been bandpass filtered (1–10 Hz) and normalized with respect to its own maximum amplitude. The reduction velocity is $6/1.732 = 3.46\text{ km s}^{-1}$, and the timescale has also been compressed by a factor of 1.732 with respect to that for the *P* waves. Use of the factor 1.732 means that, if Poisson's ratio (σ) is everywhere 0.25, the *S*-wave phases should coincide with the *P*-wave phases when one record section is laid on the other. Conversely, if the *S*-wave and *P*-wave phases do not coincide this is a first indication that σ deviates from 0.25.

In the record section from shot-point 1 (Fig. 9), the *Sg* phase can be recognized out to distances of 100–150 km at a reduced time of about 0.5 s. A distinct reflected phase, *SmS*, from the Moho can also be seen between 120 and 210 km distance,

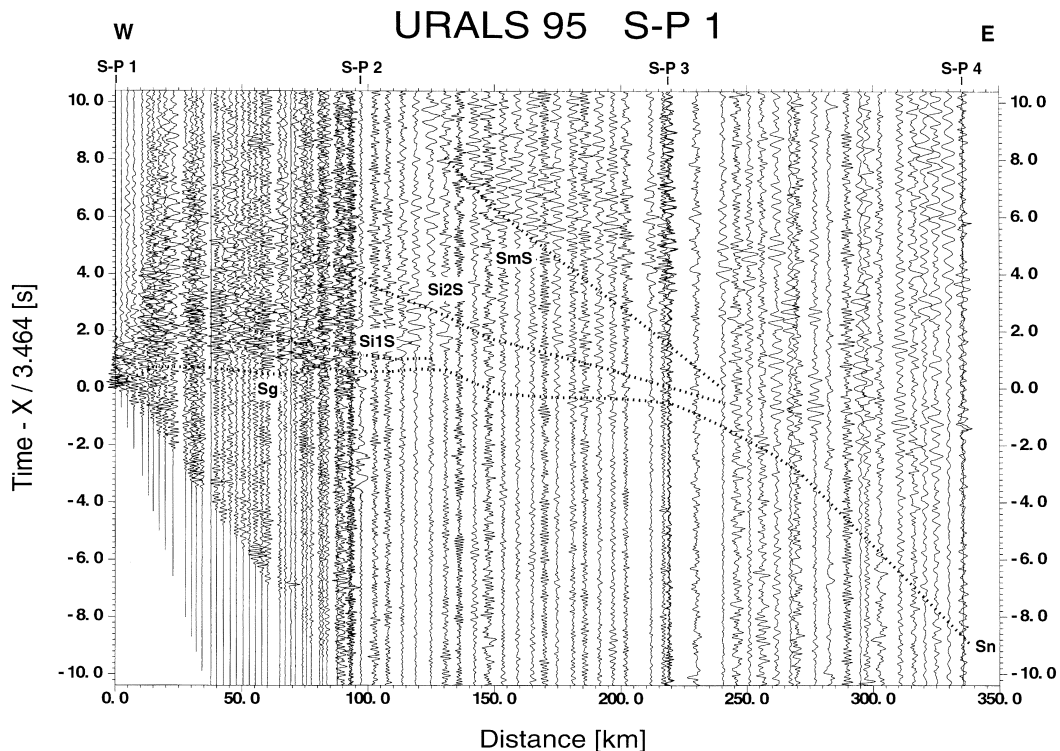


Figure 9. Seismic data from shot-point 1 along the URSEIS 95 E–W main line. The record section, reduced with a velocity of 3.464 km s^{-1} , shows the transverse component of *S*-wave motion in which each trace is normalized individually and bandpass filtered from 1 to 10 Hz. Dotted lines represent phases calculated from the model in Fig. 12. *Sg*: *S*-wave refraction through the upper crust; *Si1S*: reflection from the top of the middle crust; *Si2S*: reflection from the top of the lower crust; *SmS*: reflection from the Moho; *Sn*: *S*-wave refraction through the uppermost mantle.

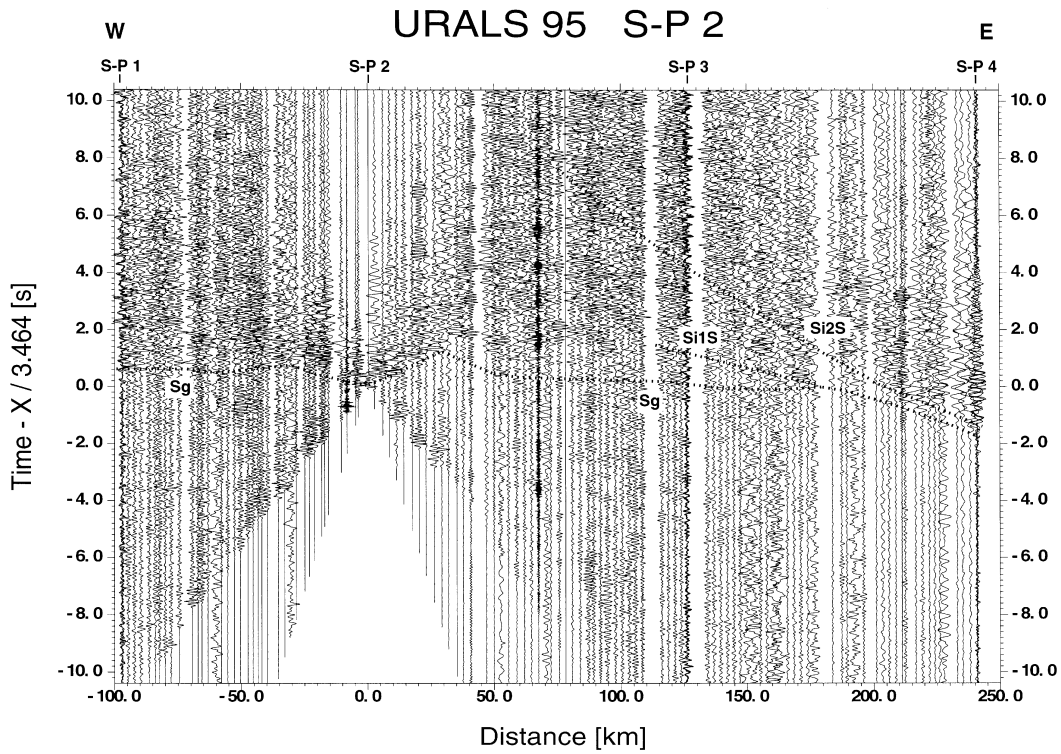


Figure 10. Transverse-component *S*-wave record section from shot-point 2 along the URSEIS 95 E–W main line. The data are processed and presented as in Fig. 9. Key: see Fig. 9.

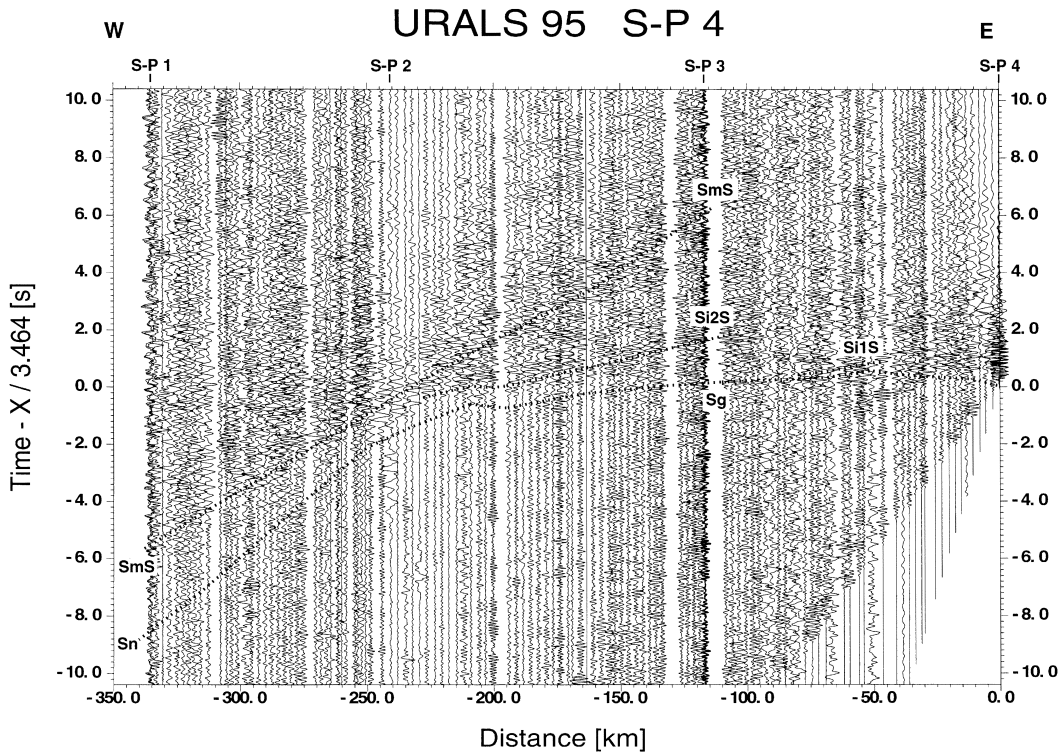


Figure 11. Transverse-component *S*-wave record section from shot-point 4 along the URSEIS 95 E–W main line. The data are processed and presented as in Fig. 9. Key: see Fig. 9.

although the *S*-wave reflection is not as bright as the *P*-wave reflection. Over most of the observation range, the horizontally polarized component of the *SmS* reflection is about 0.6 s later than would be expected if the whole crust had an average σ

of 0.25. This is thus a first indication that σ in the crust beneath the Urals is on average somewhat higher than 0.25. Intracrustal *S*-wave reflected phases are not conspicuous on this record section. They are, however, somewhat more visible

on the record section from shot-point 2 (Fig. 10), where the *Si1S* phase can be observed between 115 and 200 km distance and the *Si2S* phase is the most prominent phase beyond about 180 km distance. In this record section the *Sg* phase can be followed sporadically out to the end of the profile to the west but only out to about 30–40 km distance to the east. The most prominent phase on the *S*-wave record section from shot-point 4 (Fig. 11) is observed between 200 and 335 km distance and between 0 and -6 s reduced time. This phase is correlated as the outer part of the wide-angle reflection, *SmS*, from the Moho, and gives further confidence in the interpretation that the lower crust beneath the profile has relatively high velocities. At distances smaller than 200 km, although sharp onsets cannot be observed, energy increases associated with *SmS* and the intracrustal reflection *Si2S* can be recognized. On this record section the horizontally polarized component of the *SmS* reflected phase is about 0.7 s later than would be expected if the average crustal σ were 0.25, again indicating that the average crustal σ beneath the Urals is somewhat greater than 0.25.

S-wave model

In a first model, Poisson's ratio (σ) was assumed to be 0.25 everywhere and it was also assumed that the boundaries which exist in the *P*-wave model also exist in the *S*-wave model. In the subsequent models, including the final model (Fig. 12), the boundaries were held fixed and only the velocities in the various layers were changed. From the final *P*- and *S*-wave models a σ model was constructed (Fig. 12).

West of the Main Uralian Fault, in the West and Central Uralian zones, the 2–3 km thick upper layer with a *P*-wave velocity of around 5.5 km s^{-1} has been modelled with an *S*-wave velocity of about 3.0 km s^{-1} ($\sigma = 0.29$). The low *S*-wave velocity and high σ in this layer explain the slow *S*-wave traveltimes out to distances of about 40 km in the record section from shot-point 1 (Fig. 9). Below this layer, the layer with *P*-wave velocities of $6.0\text{--}6.1 \text{ km s}^{-1}$ has been modelled with an *S*-wave velocity of around 3.5 km s^{-1} ($\sigma = 0.24$). East of the Main Uralian Fault, in the Magnitogorsk-Tagil island arc zone, traveltimes delays in the *Sg* phase, similar to those seen for the *Pg* phase, can be recognized in the record sections from shot-points 1–3 (Figs 9 and 10). Thus, for *S*-waves also, the structure in this zone can be approximated by a central block with a lower velocity of about 3.0 km s^{-1} ($\sigma = 0.26$) flanked by two blocks with higher velocities of $3.3\text{--}3.5 \text{ km s}^{-1}$ ($\sigma = 0.25\text{--}0.26$), with all three blocks being underlain by a unit with a velocity of 3.6 km s^{-1} ($\sigma = 0.25$). The Dzshabic granite in the East Uralian zone has been modelled with an *S*-wave velocity of around 3.4 km s^{-1} ($\sigma = 0.26$). East of the Troitsk Fault in the Trans Uralian zone the thin cover layer has an *S*-wave velocity of about 3.1 km s^{-1} ($\sigma = 0.21$), while the upper crust has been modelled with an *S*-wave velocity of 3.4 km s^{-1} ($\sigma = 0.26$) at the top increasing slightly to 3.5 km s^{-1} ($\sigma = 0.26$) at the bottom.

The top of the middle crust has been modelled with an *S*-wave velocity varying from about 3.6 km s^{-1} ($\sigma = 0.24\text{--}0.25$) at the ends of the profile to about 3.7 km s^{-1} ($\sigma = 0.25$) in the middle of the profile. A small velocity increase with depth results in *S*-wave velocities at the base of the middle crust varying from around 3.7 km s^{-1} ($\sigma = 0.25$) at the ends to around 3.8 km s^{-1} ($\sigma = 0.26$) in the middle of the profile. At

the top of the lower crust, the *S*-wave velocity varies from about 3.9 km s^{-1} at the ends to about 4.1 km s^{-1} in the middle of the profile, while at the base of the crust the *S*-wave velocity varies from around 4.1 km s^{-1} at the ends to around 4.2 km s^{-1} in the middle of the profile. This results in a σ of 0.26 in the eastern half of the profile and 0.27–0.28 in the western half of the profile. As *Sn* was not observed on any of the record sections, the uppermost mantle has been assigned an *S*-wave velocity of $4.6\text{--}4.7 \text{ km s}^{-1}$ ($\sigma = 0.25$).

S-wave arrivals can be picked to within ± 0.1 s at best, and often only to within ± 0.2 s. This means that *S*-wave velocities are generally only accurate to within $\pm(0.2\text{--}0.3) \text{ km s}^{-1}$. In determining the accuracy of σ , if the *P*-wave velocity estimate is 0.1 km s^{-1} too large and the *S*-wave velocity estimate is 0.1 km s^{-1} too small then this combination of errors alone will result in an error in the value of σ of 0.03 . ± 0.03 encompasses the majority of values of σ estimated in this study. However, the fact that the *SmS* reflection occurs about 0.6–0.7 s later than would be expected if the average σ throughout the whole crust were 0.25 indicates that the average crustal σ is about 0.26.

THE N–S CROSS-LINE

The *P*-wave record section obtained from the vertical component of ground motion along the N–S cross-line is presented (Fig. 13) together with a 1-D *P*-wave velocity–depth function derived from a traveltimes analysis of the observed arrivals. The weak first arrivals have an apparent velocity close to 6.1 km s^{-1} out to the maximum recording distance of 170 km and result from the *Pg* phase propagating as a diving wave through the uppermost layer of the crust. In addition to the first arrivals, two reflected phases, *Pi1P* and *Pi2P*, can be observed. They are reflected from discontinuities at 17 and 33 km depth, respectively. In this record section the increased energy level associated with the *Pi2P* phase continues for several seconds behind the phase and thus no reflected phase from the Moho can be observed. In this respect this record section is similar to the record sections on the E–W main line from shot-points 2 and 3, in which the *PmP* phase cannot be observed. The N–S line crosses the eastern fan profile at about 110–120 km distance. The reflected phase from the Moho cannot be observed on the fan profiles either, and for this reason they are not presented here. The N–S cross-line crosses the E–W main line at about 55 km distance along the N–S line and at about 200 km distance along the E–W line. The discontinuities at 17 and 33 km depth identified along the N–S line probably correspond to those modelled at 18 and 34 km depth, respectively, along the E–W line.

DISCUSSION AND SUMMARY

Where near-vertical incidence and wide-angle seismic data sets have been collected along the same traverse, comparison has often been made with respect to the Moho depths obtained from the two data sets (see, for example Mooney & Brocher 1987 for a global review; Barton *et al.* 1984; Gajewski & Prodehl 1987; Deemer & Hurich 1991; Jones *et al.* 1996). For the wide-angle data set described here, normal incidence two-way traveltimes have been calculated for the Moho at a number of points along the E–W main line. A comparison between these traveltimes and traveltimes read from the stacked section from the near-vertical incidence explosive source survey

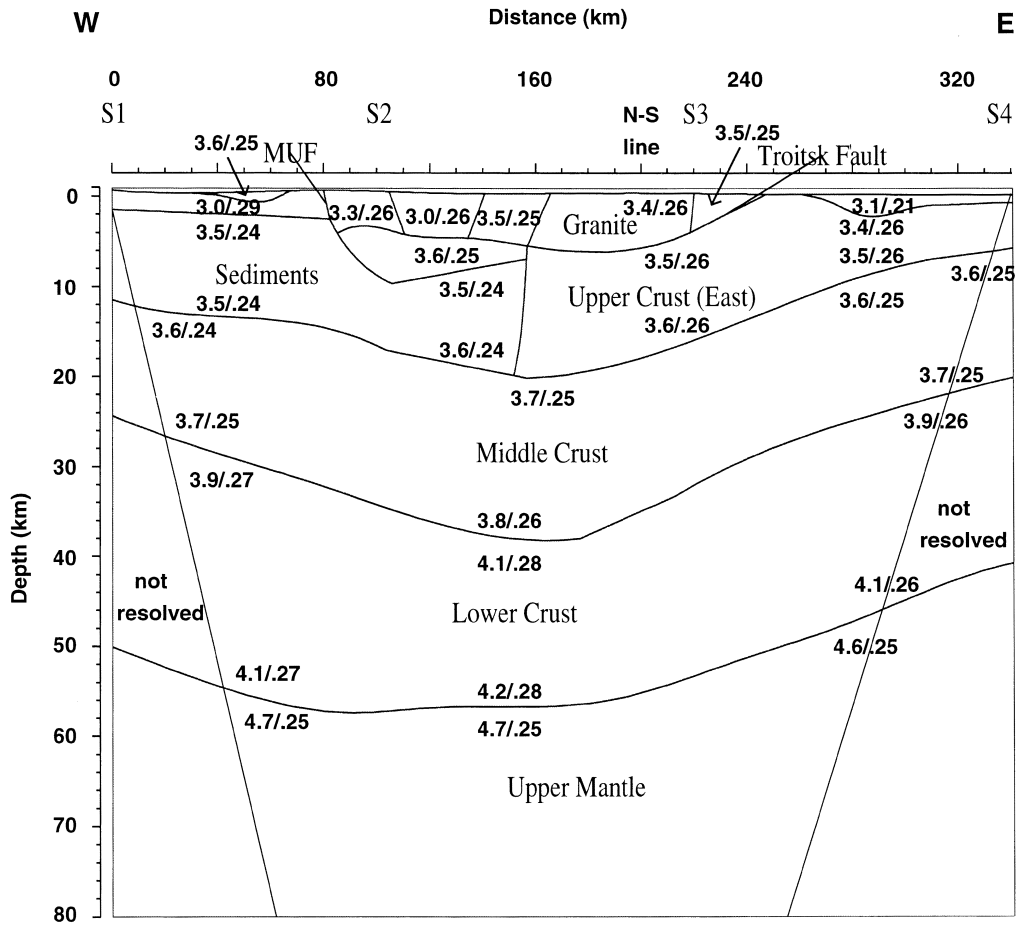


Figure 12. S-wave velocity and Poisson's ratio model for the E-W main line. Velocities are in km s^{-1} . S1-S4: shot-points S1-S4. MUF: Main Uralian Fault.

(Knapp *et al.* 1996) shows the traveltimes derived from the two data sets to agree to within 1 s or about 3 km in depth. This agreement gives confidence that the two data sets are in fact imaging the same structural interface. This is the conclusion that has been drawn for several other comparisons of similar data sets (for example Barton *et al.* 1984; Klemperer *et al.* 1986; Gajewski & Prodehl 1987; Deemer & Hurich 1991) although, as Jones *et al.* (1996) point out, even a 0.5 s mismatch may indicate up to 5 per cent difference in vertical and horizontal velocities and thus significant crustal-scale anisotropy.

The results obtained from the URSEIS wide-angle seismic data can be compared with other profiles crossing the Urals and published in the western literature. Based on Russian seismic refraction and wide-angle reflection profiles Ryzhiy *et al.* (1992) published a map of crustal thicknesses which shows a crustal root of 10–15 km associated with the Urals from 50°N to 68°N, or more or less along the whole length of the orogen. The 4000 km long Peaceful Nuclear Explosion (PNE) profile Quartz crosses the northern Urals at about 64°N. Here there is evidence for a 10–12 km thick crustal root beneath the Urals (Egorkin & Mikhaltsev 1990; Ryberg *et al.* 1996). In the middle Urals at about 58°N the 55 km long ESRU deep seismic reflection profile crosses the Main Uralian Fault about half-way along its length. Tectonic models with and without a crustal root have been proposed to explain the data from this profile (Juhlin *et al.* 1995). At about the same

latitude a 175 km long wide-angle reflection fan profile revealed a crustal root of about 6 km beneath this part of the orogen (Thouvenot *et al.* 1995).

Based on the sections derived from the near-vertical incidence reflection surveys, Berzin *et al.* (1996) presented a whole-crust structural model through the orogen along the E-W main line. Within the framework of this model the crustal root beneath the Magnitogorsk-Tagil zone with its associated high velocities would belong to the footwall of the Main Uralian Fault and thus to the lower Russian plate, which was underthrust below the upper Siberian plate.

The Bouguer anomaly across the Urals at the latitude of the E-W main line consists of an approximately 50 mgal positive anomaly 100–150 km wide and centred on the Magnitogorsk zone, superimposed on an approximately 50 mgal negative anomaly about 500 km in width also centred more or less on the Magnitogorsk zone where the crust reaches its greatest thickness (Döring *et al.* 1997). The negative anomaly is due, at least in part, to the crustal root. In fact, a 15–18 km thick crustal root produces too big an anomaly. Utilizing the Bouguer slab formula (Dobrin & Savit 1988) and assuming a 0.3 g cm^{-3} density contrast at the Moho results in an anomaly of about -200 mgal . One way to reduce the size of the minimum caused by the crustal root is to invoke a high-density (high-velocity) body at the base of the crustal root with a density contrast with respect to the uppermost mantle of about

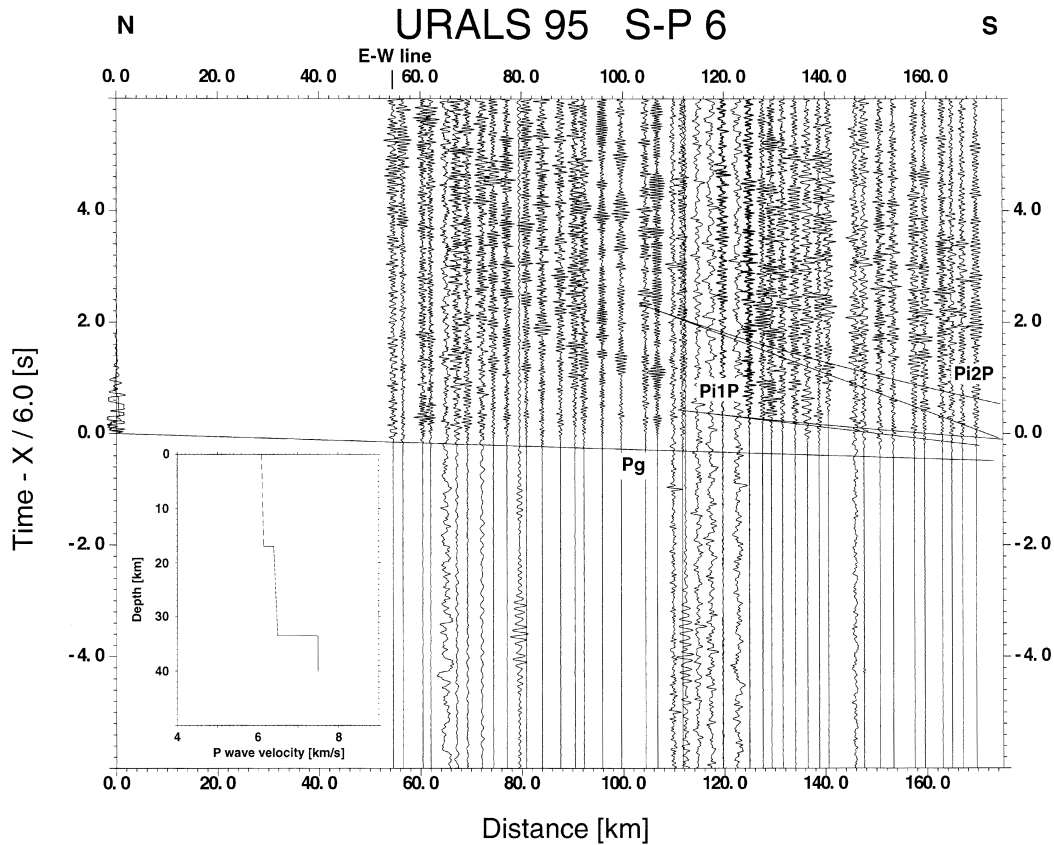


Figure 13. Seismic data and 1-D P -wave velocity-depth function for shot-point 6 along the URSEIS 95 N-S cross-line. The record section, reduced with a velocity of 6 km s^{-1} , shows the vertical component of P -wave motion in which each trace is normalized individually and bandpass filtered from 1 to 20 Hz. Continuous lines represent phases calculated from the velocity-depth function in the inset. Key: see Fig. 2.

-0.1 g cm^{-3} , as utilized by Döring *et al.* (1997). The positive anomaly has been interpreted to be due to a high-density body in the crust (Kruse & McNutt 1988) and, more recently, Döring *et al.* (1997) have modelled the high-density body as occurring for about 100 km east of the Main Uralian Fault between 3 and 10 km depth. This more or less coincides with the position of the 6.3 km s^{-1} high-velocity body at 4–9 km depth beneath the Magnitogorsk zone in the velocity model (Fig. 7).

To try to quantify the nature of the high-velocity bodies, a data bank containing velocity measurements for 416 rocks of many different types compiled from Birch (1960), Bonatti & Seyler (1987), Christensen (1965, 1966a, 1966b, 1972, 1974, 1977, 1978, 1979), Christensen & Fountain (1975), Christensen & Shaw (1970), Fountain (1976), Hall & Simmons (1979), Kanamori & Mizutani (1965), Kern (1982), Kern & Schenk (1985), Manghnani *et al.* (1974), Simmons (1964) and Simmons & Brace (1965) was searched and the results compared with the seismic velocities. One possible problem, especially for the basal crustal body, is the temperature at lower crustal depths. To circumvent this problem for the lower crustal high-velocity body ($7.3\text{--}7.5 \text{ km s}^{-1}$), the data bank was searched for a temperature of about 300°C at 55 km depth and a temperature of about 850°C at 55 km depth. These temperatures encompass the range of temperatures proposed by Kukkonen *et al.* (1997) from surface heat-flow data for this depth beneath the Magnitogorsk zone. It turns out that in both cases rocks of mafic composition such as eclogite containing rather small amounts of pyroxene and garnet (Birch 1960), amphibolite,

granofels, pyriclasite, metagabbro or gabbro are the most likely candidates to explain the lower crustal high-velocity body. If the requirement for high density is to be met then amphibolite and eclogite are the most attractive candidates. However, amphibolite should be converted to eclogite at such high pressures and thus can probably be ruled out.

The above discussion assumes a single rock type to explain the measured seismic velocities. However, a mixture of rock types could also be invoked to explain the velocities. For example, a mixture of 50 per cent mantle rocks such as peridotite with a velocity of around $8.0\text{--}8.1 \text{ km s}^{-1}$ and 50 per cent mafic crustal rocks such as gabbro with a velocity of about 6.8 km s^{-1} would result in a velocity of about $7.4\text{--}7.5 \text{ km s}^{-1}$. In this case, the crust and mantle rock types would have to be very intimately mixed. Otherwise, the seismic waves from the wide-angle experiment with frequencies of a few hertz and those from the near-vertical incidence experiment with frequencies up to about 20 Hz would detect the Moho if the individual bodies of mantle rock types were large enough. A mixture of crustal and mantle rocks forming the crustal root has already been hinted at by Juhlin *et al.* (1995) as one possible tectonic model to explain the deep seismic reflection data from the ESRU profile across the middle Urals about 500 km north of the URSEIS profile.

In the case of the upper crustal high-velocity body, rocks of almost any type can be found with a velocity of about 6.3 km s^{-1} at 4–9 km depth. If this body should contribute to the positive Bouguer gravity anomaly then a rock type with a

high density would be the most obvious choice. Rock types with the required velocity and high density ($>2.9 \text{ g cm}^{-3}$ as used by Döring *et al.* 1997) include metagabbro, serpentinized peridotite and amphibolite and metapelite of mafic composition. Geologically, the Magnitogorsk zone is a synformal structure in which mafic rock types of island arc and oceanic affinity are dominant (Hamilton 1970; Zonenshain *et al.* 1984; Kukkonen *et al.* 1997). The zone is also characterized by a surface heat-flow minimum of around 30 mW m^{-2} to which the main contributing factor is the low level of crustal radiogenic heat production (Kukkonen *et al.* 1997). This, in turn, implies that the rocks of the zone are of basic rather than acidic composition (see, for example, Telford *et al.* 1990). Thus the interpretation of the upper crustal high-velocity body as consisting of rocks of mafic and/or ultramafic composition would satisfy the constraints imposed by seismic velocity, gravity, surface heat-flow and geology.

In summary, the results obtained from *P*- and *S*-wave modelling of the data obtained during the seismic refraction-wide-angle reflection experiment of the URSEIS95 seismic project demonstrate the presence of a 15–18 km thick crustal root beneath the Magnitogorsk-Tagil zone in the central part of the orogen. However, it should be noted that the centre of this crustal root is displaced by 50–80 km to the east of the present-day maximum topography. Also beneath the Magnitogorsk-Tagil zone, an upper crustal body with a high *P*-wave velocity of 6.3 km s^{-1} at 4–9 km depth can be interpreted as consisting of mafic and/or ultramafic rocks. This, in turn, would help to explain the positive Bouguer gravity anomaly and the surface heat-flow minimum associated with the zone and would also be consistent with the known surface geology of the zone. Another major feature of the seismic model is the presence of high *P*- and *S*-wave velocities (7.5 and 4.2 km s^{-1} , respectively) at the base of the crustal root. If the base of the root also has high densities (small density contrast of about -0.1 g cm^{-3} with respect to the uppermost mantle) then this helps to explain the absence of a pronounced gravity minimum associated with the root. These high velocities and densities at the base of the thickened crust can be most easily explained by mafic rocks or a mix of mafic and ultramafic rocks. Within the structural framework of Berzin *et al.* (1996) these rocks would belong to the lower Russian plate which was being subducted beneath the Siberian plate during the Uralian orogeny. It is attractive to speculate that the crustal root is the remnants of oceanic crust or a mix of oceanic crust and mantle attached to the Russian plate. This, in turn, would mean that little or no continental crust has been subducted or that subduction, and hence the Uralian orogeny, stopped when there was no more oceanic crust or when an attempt was made to subduct lighter continental crust.

ACKNOWLEDGMENTS

The help of many scientists, technicians and students from Spain, Russia, USA and Germany during the fieldwork is acknowledged. Funding for this project was provided by the German Federal Ministry of Science and Technology (BMBF) through grant 03GT94101 to the DEKORP 2000 program, the German Science Foundation (DFG), Comisión Interministerial de Ciencia y Tecnología (AMB 95–0987E), the Continental Dynamics Program (NSF grant EAR-9418251 to Cornell University), ROSCOMNEDRA and the International

Association for the Cooperation with Scientists from the Former Soviet Union (grant 94–1857). The project was supported by the GeoForschungsZentrum Potsdam and forms part of EUROPROBE's Urals project. The recording instruments were provided by the geophysical instrument pool of the GeoForschungsZentrum (GFZ) Potsdam (40 REFTEKs) and the Instituto de Ciencias de la Terra Jaume Almera (ICTJA), CSIC-Barcelona (10 MARS). Data processing was carried out using ProMAX from Advance Geophysical Corporation, while ray-tracing was carried out using the facility in the GX II (GX II is a Trademark of GX Technology Corporation) commercial software modelling package. The finite-difference traveltimes and amplitude calculations were performed on the CONVEX Exemplar SPP1000 computer of the central computing facility at the GFZ Potsdam.

REFERENCES

- Aichroth, B., Prodehl, C. & Thybo, H., 1992. Crustal structure along the central segment of the EGT from seismic-refraction studies, in *The European Geotraverse, Part 8*, eds Freeman, R. & Mueller, St., *Tectonophysics*, **207**, 43–64.
- Barton, P.J., Matthews, D., Hall, J. & Warner, M., 1984. Moho beneath the North Sea compared on normal incidence and wide-angle seismic records, *Nature*, **308**, 55–56.
- Berzin, R., Oncken, O., Knapp, J.H., Pérez-Estaún, A., Hismatulin, T., Yunusov, N. & Lipilin, A., 1996. Orogenic evolution of the Ural mountains: Results from an integrated seismic experiment, *Science*, **274**, 220–221.
- Birch, F., 1960. The velocity of compressional waves in rocks to 10 kilobars, 1. *J. geophys. Res.*, **65**, 1083–1102.
- Bois, C., 1991. Geological significance of seismic reflections in collision belts, *Geophys. J. Int.*, **105**, 55–69.
- Bonatti, E. & Seyler, M., 1987. Crustal underplating and evolution in the Red Sea Rift: Uplifted gabbro/gneiss crustal complexes on Zabargad and Brothers Islands, *J. geophys. Res.*, **92**, 12 803–12 821.
- Brown, D., Puchkov, V., Alvarez-Marrón, J. & Pérez-Estaún, A., 1996. The structural architecture of the footwall to the Main Uralian Fault, southern Urals, *Earth Sci. Rev.*, **40**, 125–147.
- Carbonell, R., Pérez-Estaún, A., Gallart, J., Diaz, J., Kashubin, S., Mechie, J., Stadtlander, R., Schulze, A., Knapp, J.H. & Morozov, A., 1996. Crustal root beneath the Urals: Wide-angle seismic evidence, *Science*, **274**, 222–224.
- Christensen, N.I., 1965. Compressional wave velocities in metamorphic rocks at pressures to 10 kilobars, *J. geophys. Res.*, **70**, 6147–6164.
- Christensen, N.I., 1966a. Shear wave velocities in metamorphic rocks at pressures to 10 kilobars, *J. geophys. Res.*, **71**, 3549–3556.
- Christensen, N.I., 1966b. Elasticity of ultrabasic rocks, *J. geophys. Res.*, **71**, 5921–5931.
- Christensen, N.I., 1972. Compressional and shear wave velocities at pressures to 10 kilobars for basalts from the East Pacific Rise, *Geophys. J. R. astr. Soc.*, **28**, 425–429.
- Christensen, N.I., 1974. Compressional wave velocities in possible mantle rocks to pressures of 30 kbar, *J. geophys. Res.*, **79**, 407–412.
- Christensen, N.I., 1977. The geophysical significance of oceanic plagiogranite, *Earth planet. Sci. Lett.*, **36**, 297–300.
- Christensen, N.I., 1978. Ophiolites, seismic velocities, and oceanic crustal structure, *Tectonophysics*, **47**, 131–157.
- Christensen, N.I., 1979. Compressional wave velocities in rocks at high temperatures and pressures, critical thermal gradients, and crustal low-velocity zones, *J. geophys. Res.*, **84**, 6849–6857.
- Christensen, N.I. & Fountain, D.M., 1975. Constitution of the lower continental crust based on experimental studies of seismic velocities in granulite, *Geol. Soc. Am. Bull.*, **86**, 227–236.
- Christensen, N.I. & Shaw, G.H., 1970. Elasticity of mafic rocks

- from the Mid-Atlantic Ridge, *Geophys. J. R. astr. Soc.*, **20**, 271–284.
- Cook, F., Brown, L., Kaufman, S., Oliver, J. & Peterson, T., 1981. COCORP seismic profiling of the southern Appalachian orogen beneath the Coastal Plain of Georgia, *Geol. Soc. Am. Bull.*, **92**, 738–748.
- Deemer, S.J. & Hurich, C.A., 1991. Comparison of coincident high-resolution wide-aperture and CDP profiling along the southwest coast of Norway, *Am. geophys. Un. Geodyn. Ser.*, **22**, 435–442.
- Dobrin, M.B. & Savit, C.H., 1988. *Introduction to Geophysical Prospecting*, 4th edn, McGraw-Hill, New York.
- Döring, J., Götzte, H.-J. & Kaban, M., 1997. Preliminary study of the gravity field of the southern Urals along the URSEIS '95 seismic profile, in *Europrobe's Urals Project*, eds Pérez-Estaún, A., Brown, D. & Gee, D., *Tectonophysics*, **276**, 49–62.
- Echtler, H.P., Stiller, M., Steinhoff, F., Krawczyk, C., Suleimanov, A., Spiridonov, V., Knapp, J.H., Menshikov, Y., Alvarez-Marrón, J. & Yunusov, N., 1996. Preserved collisional crustal structure of the Southern Urals revealed by vibroseis profiling, *Science*, **274**, 224–226.
- Egorkin, A.V. & Mikhaltsev, A.V., 1990. The result of seismic investigations along geotraverses, in *Super-Deep Continental Drilling and Deep Geophysical Sounding*, pp. 111–119, eds Fuchs, K., Kozlovsky, Ye.A., Krivtsov, A.I. & Zoback, M.D., Springer-Verlag, Berlin.
- Fountain, D.M., 1976. The Ivrea-Verbano and Strona-Ceneri Zones, northern Italy: a cross-section of the continental crust—New evidence from seismic velocities of rock samples, *Tectonophysics*, **33**, 145–165.
- Gajewski, D. & Prodehl, C., 1987. Seismic Refraction Investigation of the Black Forest, in *The European Geotraverse, Part 3*, eds Freeman, R. & Mueller, St., *Tectonophysics*, **142**, 27–48.
- Hall, J. & Simmons, G., 1979. Seismic velocities of Lewisian metamorphic rocks at pressures to 8 kbar: Relationship to crustal layering in North Britain, *Geophys. J. R. astr. Soc.*, **58**, 337–347.
- Hamilton, W., 1970. The Uralides and the motion of the Russian and Siberian platforms, *Geol. Soc. Am. Bull.*, **81**, 2553–2576.
- Jones, K.A., Warner, M.R., Morgan, R.P., Morgan, J.V., Barton, P.J. & Price, C.E., 1996. Coincident normal-incidence and wide-angle reflections from the Moho: evidence for crustal seismic anisotropy, in *Seismic Reflection Probing of the Continents and Their Margins*, eds White, D.J., Ansorge, J., Bodoky, T.J. & Hajnal, Z., *Tectonophysics*, **264**, 205–217.
- Juhlin, C., Kashubin, S., Knapp, J.H., Makovsky, V. & Ryberg, T., 1995. Project conducts seismic reflection profiling in the Ural mountains, *EOS, Trans. Am. geophys. Union*, **76**, 197–199.
- Kanamori, H. & Mizutani, H., 1965. Ultrasonic measurements of elastic constants of rocks under high pressures, *Bull. Earthquake Res. Inst. University of Tokyo*, **43**, 173–194.
- Kelly, K.R., Ward, R.W., Treitel, S. & Alford, R.M., 1976. Synthetic seismograms: a finite-difference approach, *Geophysics*, **41**, 2–27.
- Kern, H., 1982. P- and S-wave velocities in crustal and mantle rocks under the simultaneous action of high confining pressure and high temperature and the effect of rock microstructure, in *High-Pressure Researches in Geoscience*, pp. 15–45, ed. Schreyer, W., Schweizerbart, Stuttgart.
- Kern, H. & Schenk, V., 1985. Elastic wave velocities in rocks from a lower crustal section in southern Calabria (Italy), *Phys. Earth planet. Inter.*, **40**, 147–160.
- Klemperer, S.L., Hauge, T.A., Hauser, E.C., Oliver, J.E. & Potter, C.J., 1986. The Moho in the northern Basin and Range province, Nevada, along the COCORP 40°N seismic-reflection transect, *Geol. Soc. Am. Bull.*, **97**, 603–618.
- Knapp, J.H., Steer, D.N., Brown, L.D., Berzin, R., Suleimanov, A., Stiller, M., Lüschen, E., Brown, D.L., Bulgakov, R., Kashubin, S.N. & Rybalka, A.V., 1996. Lithosphere-scale seismic image of the Southern Urals from explosion-source reflection profiling, *Science*, **274**, 226–228.
- Kruse, S. & McNutt, M., 1988. Compensation of Paleozoic orogens: a comparison of the Urals to the Appalachians, *Tectonophysics*, **154**, 1–17.
- Kukkonen, I.T., Golovanova, I.V., Khachay, Yu.V., Druzhinin, V.S., Kosarev, A.M. & Schapov, V.A., 1997. Low geothermal heat flow of the Urals fold belt—implication of low heat production, fluid circulation or palaeoclimate? in *Europrobe's Urals Project*, eds Pérez-Estaún, A., Brown, D. & Gee, D., *Tectonophysics*, **276**, 63–85.
- Manghnani, M.H., Ramanantoandro, R. & Clark, S.P. Jr, 1974. Compressional and shear wave velocities in granulite facies rocks and eclogites to 10 kbar, *J. geophys. Res.*, **79**, 5427–5446.
- Mooney, W.D. & Brocher, T.M., 1987. Coincident seismic reflection/refraction studies of the continental lithosphere: a global review, *Rev. Geophys.*, **25**, 723–742.
- Nelson, K.D., 1992. Are crustal thickness variations in old mountain belts like the Appalachians a consequence of lithospheric delamination?, *Geology*, **20**, 498–502.
- Podvin, P. & Lecomte, I., 1991. Finite difference computation of traveltimes in very contrasted velocity models: a massively parallel approach and its associated tools, *Geophys. J. Int.*, **105**, 271–284.
- Reynolds, A.C., 1978. Boundary conditions for the numerical solution of wave propagation problems, *Geophysics*, **43**, 1099–1110.
- Ryberg, T., Wenzel, F., Mechie, J., Egorkin, A., Fuchs, K. & Solodilov, L., 1996. Two-dimensional velocity structure beneath northern Eurasia derived from the super long-range seismic profile Quartz, *Bull. seism. Soc. Am.*, **86**, 857–867.
- Ryzhiy, B.P., Druzhinin, V.S., Yunusov, F.F. & Ananyin, I.V., 1992. Deep structure of the Urals region and its seismicity, *Phys. Earth planet. Inter.*, **75**, 185–191.
- Sandmeier, K.-J., 1990. Untersuchung der Ausbreitungseigenschaften seismischer Wellen in geschichteten und streuenden Medien, *PhD thesis*, Karlsruhe University.
- Schneider, W.A., Ranzinger, K.A., Balch, A.H. & Kruse, C., 1992. A dynamic programming approach to first arrival traveltime computation in media with arbitrarily distributed velocities, *Geophysics*, **57**, 39–50.
- Simmons, G., 1964. Velocity of shear waves in rocks to 10 kilobars, *J. geophys. Res.*, **69**, 1123–1130.
- Simmons, G. & Brace, W.F., 1965. Comparison of static and dynamic measurements of compressibility of rocks, *J. geophys. Res.*, **70**, 5649–5656.
- Telford, W.M., Geldart, L.P. & Sheriff, R.E., 1990. *Applied Geophysics*, 2nd edn, Cambridge University Press, Cambridge.
- Thouvenot, F., Kashubin, S.N., Poupinet, G., Makovskiy, V.V., Kashubina, T.V., Matte, Ph. & Jenatton, L., 1995. The root of the Urals: evidence from wide-angle reflection seismics, *Tectonophysics*, **250**, 1–13.
- Vidale, J., 1988. Finite-difference calculation of travel times, *Bull. seism. Soc. Am.*, **78**, 2062–2076.
- Zonenshain, L.P., Korinevsky, V.G., Kazmin, V.G., Pechersky, D.M., Khain, V.V. & Matveenkov, V.V., 1984. Plate tectonic model of the South Urals development, in *Appalachian and Hercynian Fold Belts*, eds Zwart, H.J., Behr, H.-J. & Oliver, J.E., *Tectonophysics*, **109**, 95–135.